Operation of distribution networks integrated with hybrid energy storage systems

Nguyen Thi Anh[1], Pham Nang Van[2*]

[1]*Power Grid and Renewable Energy Lab (PGRE), School of Electrical and Electronic Engineering, Hanoi University of Science and Technology*
[2]*School of Electrical and Electronic Engineering, Hanoi University of Science and Technology*
[*]*Corresponding author E-mail: van.phamnang@hust.edu.vn*
DOI: https://doi.org/10.64032/mca.v30i2.423

Abstract

This paper proposes an optimization model to minimize the operating costs of a modern power distribution network integrated with distributed generation (DG), battery energy storage systems (BESS), and hydrogen energy storage systems (HESS). The objective of the proposed model is to minimize the cost of electricity purchased from the transmission grid. The optimization problem is formulated as a mixed-integer second-order cone programming (MISOCP) model, derived from a mixed-integer nonlinear programming (MINLP) formulation via second-order cone representations of the power flow equations. The model is implemented in GAMS using the commercial solver GUROBI and tested on a modified IEEE 33-bus distribution network. The calculation results show the effectiveness of the proposed optimization formulation.

Keywords: *Power distribution grids; Battery energy storage systems; Hydrogen energy storage systems; Mixed-integer second-order cone programming; Distributed generation.*

Symbols

Symbols	Units	Description
Φ_i		Group of buses directly connected to bus *i*
Φ_{L}		Group of branches
Φ_{N}		Group of nodes in the network
Ω_{HESS}		Set of buses where HESS is installed
Ω_{BESS}		Set of buses where BESS is installed
S_{base}	MVA	Base power
r		Discount rate
t	hour	Time index of the day
Δt	hour	Calculation time step
N	year	Lifetime of the energy storage system
$c_{i,t}^{sub}$	\$/MWh	Electricity price
$P_{i,t}^{sub}$	p.u.	Power purchased from the transmission grid
$P_{i,t}^{\mathrm{DG}}$, $Q_{i,t}^{\mathrm{DG}}$	p.u.	Active and reactive power of the DG at bus *i* at time *t*
$P_{i,t}^{\mathrm{D}}$, $Q_{i,t}^{\mathrm{D}}$	p.u.	Active and reactive powers of the load at bus *i* at time *t*
$P_{ij,t}$, $Q_{ij,t}$	p.u.	Active and reactive power flows on branch *ij* at time *t*
$I_{ij,t}$	p.u.	Current value on line *ij* at time *t*
$I_{ij,\max}$	p.u.	Maximum allowable current value on line *ij*
U_i	p.u.	Voltage magnitude at bus *i*
$U_{i,\min}$	p.u.	Lower voltage limit at bus *i*
$U_{i,\max}$	p.u.	Upper voltage limit at bus *i*
R_{ij}	p.u.	Resistance on branch *ij*
X_{ij}	p.u.	Reactance on branch *ij*
$m_{i,t}^{\mathrm{EL}}$		Hydrogen mass
$P_{i,t}^{\mathrm{EL}}$	p.u.	Electric power
η_i^{EL}		Efficiency of the HESS electrolysis process at bus *i*
$u_{i,t}^{\mathrm{EL}}$		Binary variable $u_{i,t}^{\mathrm{EL}}=1$ when the electrolyzer is operating, and otherwise, $u_{i,t}^{\mathrm{EL}}=0$
α_i^{EL}		Ratio of the minimum operating power to the installed capacity of the electrolyzer at bus *i*
LHV_i	$\mathrm{Wh/Nm^3}$	Conversion coefficient between hydrogen mass and electrical energy
$m_{i,t}^{\mathrm{HT,in}}$	$\mathrm{Nm^3/h}$	Mass of H2 supplied to the storage tank at bus *i* at time *t*
$m_{i,t}^{\mathrm{HT,out}}$	$\mathrm{Nm^3/h}$	Mass of H2 extracted to the storage tank at bus *i* at time *t*
$m_{i,t}^{\mathrm{HT}}$	$\mathrm{Nm^3}$	Mass of H2 in the storage tank at bus *i* at time *t*
$\eta^{\mathrm{HT,in}}$ $\eta^{\mathrm{HT,out}}$		Charging and discharging efficiency of the storage tank
$\gamma_{\mathrm{loss,HT}}$		Self-discharge loss of the storage tank

Received: 8 March 2026; Revised: 24 March 2026; Accepted: 18 April 2026.

$m_i^{\mathrm{HT,min}}$		Minimum and maximum mass of H2 in the storage tank at bus *i*
$m_i^{\mathrm{HT,max}}$		
α_i^{HT}		Ratio between the minimum capacity and the installed capacity of the hydrogen storage tank
$C_{ref,i}^{\mathrm{HT}}$		Installed capacity of the hydrogen storage tank
$P_{i,t}^{\mathrm{FC}}$	p.u.	Electrical power in the fuel cell
η_i^{FC}		Electrical efficiency of the fuel cell
$u_{i,t}^{\mathrm{FC}}$		Binary variable, $u_{i,t}^{\mathrm{FC}}=1$ when the fuel cell is operating, and otherwise, $u_{i,t}^{\mathrm{FC}}=0$
$E_{i,t}^{\mathrm{BESS}}$	p.u.	Energy level of BESS at node *i* at time *t*
$E_{i,0}^{\mathrm{BESS}}$	p.u.	Initial energy level of BESS at node *i*
$E_{\mathrm{max},i}^{\mathrm{BESS}}$	p.u.	Maximum energy level of BESS at node *i*
α_i^{BESS}		Ratio between the minimum and maximum energy levels of BESS at bus *i*
$P_{i,t}^{\mathrm{BESS,ch}}$	p.u.	Charge/discharge power of BESS at node *i* at time *t*
$P_{i,t}^{\mathrm{BESS,dis}}$		
$\eta_i^{\mathrm{BESS,ch}}$		Charging and discharging efficiencies of BESS at node *i* at time *t*
$\eta_i^{\mathrm{BESS,dis}}$		
$P_{\mathrm{max},i}^{\mathrm{BESS}}$	p.u.	Peak charging/ discharging power of BESS at node *i* at time *t*
$v_{i,t}^{\mathrm{BESS}}$		Binary variable, $v_{i,t}^{\mathrm{BESS}}=1$ when the storage device is charging at time *t*, and otherwise, $v_{i,t}^{\mathrm{BESS}}=0$

Abbreviations

DG	Distributed generation
BESS	Battery energy storage systems
HESS	Hydrogen energy storage systems
FC	Fuel Cell
EL	Electrolyzer
HST	Hydrogen Storage Tank
MG	Microgrid
PV	Photovoltaic
NSGA–II	Non-Dominated Sorting Genetic Algorithm–II
PSO	Particle Swarm Optimization
GA	Genetic Algorithm
MINLP	Mixed-integer nonlinear programming
MILP	Mixed Integer Linear Programming
MISOCP	Mixed Integer Second Order Cone Programming

1. Introduction

With the advancement of smart grids and the increasing penetration of distributed generation (DG), distribution networks have undergone significant changes in structure, operation, and control. The proliferation of renewable energy sources and distributed generation can lead to technical challenges such as line overloading and voltage fluctuations. One effective solution to mitigate the drawbacks of integrating renewable energy into the grid is the utilization of battery energy storage systems (BESS) and hydrogen energy storage systems (HESS) [1]. A typical HESS consists of an electrolyzer (EL), a fuel cell (FC), and a hydrogen storage tank (HST). This hybrid energy system can store surplus power from renewable sources as electrical energy in the BESS or convert it into hydrogen via the EL for storage in the HST. When load demand exceeds the supply, electricity is discharged from the BESS or generated by the FC through the conversion of hydrogen back into electrical energy. The hybrid energy storage system (comprising both BESS and HESS) exhibits a flexible response to load variations, offers long-term energy storage capabilities, and provides high economic efficiency.

Many studies have presented various methods for integrating BESS and HESS into the power grid. Specifically, in [2], the authors proposed a multi-objective optimization algorithm, the non-dominated sorting genetic algorithm II (NSGA-II), to determine the optimal sizing and placement of BESS in distribution networks integrated with distributed generation, aiming to reduce power losses and limit voltage fluctuations. The improved NSGA-II method was verified on the IEEE 33-bus system, demonstrating superior performance compared to standard NSGA-II and particle swarm optimization (PSO). Study [3] developed a stochastic optimization model for a microgrid (MG) integrating HESS with wind and solar power to enhance power supply reliability and minimize system operational costs. The authors in [4] presented a mixed-integer nonlinear programming (MINLP) model for determining the optimal location and size of BESS in unbalanced active distribution networks, accounting for various uncertainties. Validation results on an unbalanced IEEE test system showed that the model effectively identifies the optimal BESS configuration with short computational times. Research [5] presents a hybrid optimization model combining PSO and genetic algorithm (GA) to determine the capacities of solar, wind, BESS, and HESS. The investigation, conducted on a Mediterranean island, demonstrated that combining energy storage systems in the grid yields economic benefits while maintaining a specific renewable energy penetration ratio. The authors in [6] presented a mixed-integer linear programming (MILP) model to integrate energy storage into active distribution networks, considering battery cycle life, load and photovoltaic (PV) uncertainties, as well as islanded operation modes. The method was evaluated on a 33-bus radial grid, an Indian distribution network, and a 141-bus Caracas network, proving its high efficiency and generalizability. Study [7] presents a model involving HESS combined with an MG to improve operational efficiency across various load profiles. In [8], the authors proposed a bi-

level optimization model to manage the islanded operation of an MG integrated with hydrogen refueling stations. The model was verified on a 33-bus system, showing effectiveness in significantly reducing operating costs under adverse conditions while improving overall efficiency through storage systems. In [9], the authors proposed a hybrid renewable energy system combining solar, wind, and hydrogen storage, utilizing a bi-level optimization model to minimize annual costs and power transaction amounts. Scenario simulations indicated that increasing PV and storage capacities improves system stability. Paper [10] determines the optimal sizing of a system including wind turbines, BESS, and HESS based on experimental data, with an objective function focused on minimizing total annual costs and the loss of power supply probability (LPSP). The optimal solution involves finding a set of system components with the lowest annual cost that still meets reliability requirements. Finally, paper [11] establishes optimal operational scheduling for a HESS under different economic and environmental conditions, considering renewable energy sources and demand response. The model is formulated as a MILP, aiming to minimize total grid costs, including operational costs related to HESS, PV, wind systems, and electricity purchase costs from the external grid.

The aforementioned studies have employed various optimization methods, such as GA, PSO, NSGA-II, MINLP, and MILP, to optimize energy storage systems, thereby enhancing the reliability and operational efficiency of the power grid. Heuristic algorithms such as GA, PSO, and NSGA-II can handle optimization problems with non-linear and integer variables. However, the main drawback of heuristic algorithms is that they do not guarantee finding a global optimal solution, require the selection of complex input parameters, and have significant computation time on large power grids. The MINLP method also encounters similar difficulties when finding the global optimal solution. Meanwhile, the MILP method can ensure a global optimal solution. However, this method can only solve linear optimization problems, leading to solutions with errors due to the need to apply approximation or linearization techniques. The MISOCP method can overcome the aforementioned drawbacks by finding the global optimal solution, improving computational speed, and ensuring solution accuracy.

Furthermore, a majority of these studies focus on BESS or HESS in isolation, often overlooking the coordination and interaction between these two systems and the distribution network. Therefore, the objective of this research is to develop a mixed-integer second-order cone programming (MISOCP) model for the optimal operation of distribution networks integrated with hybrid energy storage systems (BESS-HESS). This study provides the following significant contributions:

• Introduce the MINLP optimization model to solve the optimal operation problem of the distribution grid with the goal of minimizing the total cost of buying/selling electricity with the external grid while adhering to constraints such as power balance, line current not exceeding limits, node voltage within permissible thresholds, and constraints related to the hybrid energy storage system model;

• Develop the MISOCP model from the MINLP model by developing the quadratic cone formulation of the power flow equations;

• Analyze the impact of BESS operation on the optimal solution on the modified IEEE 33-bus grid.

The remainder of this paper is organized as follows. Section 2 details the mathematical formulation for the optimal operation of the hybrid energy storage system. Section 3 presents the numerical results and performance analysis on a modified IEEE 33-bus distribution system. Finally, conclusions and future research directions are presented in Section 4.

2. Mathematical formulation

2.1 Mixed-integer nonlinear programming model

2.1.1 Objective function

The objective function (1) of the optimal distribution network operation problem is to minimize the total cost of electricity transactions with the transmission grid throughout the lifetime of the energy storage system as follows.

$$\min f = \sum_{n=1}^{N}\left[\sum_{t=1}^{T=24}\sum_{i\in\Omega_{\text{sub}}} c_{i,t}^{\text{sub}} \times P_{i,t}^{\text{sub}} \times S_{\text{base}} \times 365\right] \times \frac{1}{(1+r)^n} \tag{1}$$

2.1.2 Network modeling

The power network constraints are formulated as follows:

$$P_{i,t}^{\text{sub}} + P_{i,t}^{\text{DG}} + P_{i,t}^{\text{FC}} - P_{i,t}^{\text{EL}} - P_{i,t}^{\text{D}} + P_{i,t}^{\text{BESS,dis}} - P_{i,t}^{\text{BESS,ch}} = \sum_{j\in\Phi_i, j\neq h} P_{ij,t} + R_{hi} \times I_{hi,t}^2 - P_{hi,t};\ \forall i \in \Phi_{\text{N}};\ t = 1,\ldots,T \tag{2}$$

$$Q_{i,t}^{\text{sub}} + Q_{i,t}^{\text{DG}} - Q_{i,t}^{\text{D}} = \sum_{j\in\Phi_i, j\neq h} Q_{ij,t} + X_{hi} \times I_{hi,t}^2 - Q_{hi,t};\ \forall i \in \Phi_{\text{N}};\ t = 1,\ldots,T \tag{3}$$

$$U_{i,t}^2 - U_{j,t}^2 - 2\times\left(R_{ij}P_{ij,t} + X_{ij}Q_{ij,t}\right) + (R_{ij}^2 + X_{ij}^2)I_{ij,t}^2 = 0;\ \forall ij \in \Phi_{\text{L}};\ t = 1,\ldots,T \tag{4}$$

$$I_{ij,t}^2 U_{i,t}^2 = P_{ij,t}^2 + Q_{ij,t}^2;\ \forall ij \in \Phi_{\text{L}};\ t = 1,\ldots,T \tag{5}$$

$$0 \le I_{ij,t}^2 \le I_{ij,\max}^2;\ \forall ij \in \Phi_{\text{L}};\ t = 1,\ldots,T \tag{6}$$

$$U_{i,\min}^2 \le U_{i,t}^2 \le U_{i,\max}^2;\ \forall i \in \Phi_{\text{N}};\ t = 1,\ldots,T \tag{7}$$

Constraints (2) and (3) are the power flow equations using the power summation method for radial distribution networks. Equation (4) expresses the voltage relationship between the nodes of branch *ij*. Equation (5) describes the relationship between node voltage, branch current, and branch power. The thermal limit of the branch is defined by (6), while equation (7) presents the voltage limits.

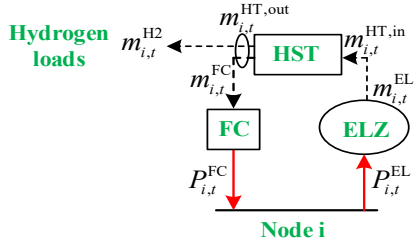

Figure 1: Hydrogen energy system at node *i*

2.1.3 Hydrogen energy storage system modeling

The hydrogen energy system (see Figure 1) consists of an electrolyzer (EL), a hydrogen storage tank, and a fuel cell (FC).

a, Electrolyzer

Alkaline electrolyzers are commonly used for hydrogen production. The relationship between the hydrogen mass $\left(m_{i,t}^{\mathrm{EL}}\right)$ and the electrical power $\left(P_{i,t}^{\mathrm{EL}}\right)$ consumed during the electrolysis process is represented as follows:

$$m_{i,t}^{\mathrm{EL}} = \frac{\eta_i^{\mathrm{EL}} \times P_{i,t}^{\mathrm{EL}}}{\mathrm{LHV}}; \quad \forall i \in \Omega_{\mathrm{HESS}}, \forall t = 1,...,T \tag{8}$$

The input electrical power of the electrolyzer at node i must satisfy the following conditions:

$$u_{i,t}^{\mathrm{EL}} \alpha_i^{\mathrm{EL}} P_{\max,i}^{\mathrm{EL}} \le P_{i,t}^{\mathrm{EL}} \le u_{i,t}^{\mathrm{EL}} P_{\max,i}^{\mathrm{EL}}; \forall i \in \Omega_{\mathrm{HESS}}, \forall t = 1,...,T \tag{9}$$

b, Hydrogen storage tank

Hydrogen (H2) produced during the electrolysis process is compressed to high pressure using a specialized compressor before being transferred to the hydrogen storage tanks (HST) for storage. In the steady state, it is assumed that all H2 produced by the electrolyzer is delivered directly to the HST. Consequently, the mass (volume) of H2 supplied to and extracted from the HESS storage tank at node i at time t is expressed as follows:

$$m_{i,t}^{\mathrm{HT,in}} = m_{i,t}^{\mathrm{EL}}; \quad \forall i \in \Omega_{\mathrm{HESS}}, \forall t = 1,...,T \tag{10}$$

$$m_{i,t}^{\mathrm{HT,out}} = m_{i,t}^{\mathrm{H2}} + m_{i,t}^{\mathrm{FC}}; \quad \forall i \in \Omega_{\mathrm{HESS}}, \forall t = 1,...,T \tag{11}$$

The mass of hydrogen in the storage tank i at time t:

$$m_{i,t}^{\mathrm{HT}} = \left(1 - \gamma_{\mathrm{loss,HT}}\right) m_{i,t-1}^{\mathrm{HT}} + \left(\eta^{\mathrm{HT,in}} m_{i,t}^{\mathrm{HT,in}} - \frac{m_{i,t}^{\mathrm{HT,out}}}{\eta^{\mathrm{HT,out}}}\right)\Delta t; \quad \forall i \in \Omega_{\mathrm{HESS}}, \forall t = 1,...,T \tag{12}$$

The constraints on the hydrogen mass limits in storage tank i at time t and the daily hydrogen volume must satisfy the following conditions:

$$m_i^{\mathrm{HT,min}} \le m_{i,t}^{\mathrm{HT}} \le m_i^{\mathrm{HT,max}}; \quad \forall i \in \Omega_{\mathrm{HESS}}, \forall t = 1,...,T \tag{13}$$

$$m_i^{\mathrm{HT,min}} = \alpha_i^{\mathrm{HT}} \times \frac{C_{ref,i}^{\mathrm{HT}}}{\mathrm{LHV}}; \quad \forall i \in \Omega_{\mathrm{HESS}} \tag{14}$$

$$m_i^{\mathrm{HT,max}} = \frac{C_{ref,i}^{\mathrm{HT}}}{\mathrm{LHV}}; \quad \forall i \in \Omega_{\mathrm{HESS}} \tag{15}$$

$$m_{i,0}^{\mathrm{HT}} = m_{i,T}^{\mathrm{HT}}; \quad \forall i \in \Omega_{\mathrm{HESS}} \tag{16}$$

$$m_{i,0}^{\mathrm{HT}} = m_i^{\mathrm{HT,min}}; \quad \forall i \in \Omega_{\mathrm{HESS}} \tag{17}$$

c, Fuel cell

The electrical power limits of the fuel cell and the relationship between its power output and hydrogen mass are as follows:

$$0 \le P_{i,t}^{\mathrm{FC}} \le u_{i,t}^{\mathrm{FC}} P_{\max,i}^{\mathrm{FC}}; \quad \forall i \in \Omega_{\mathrm{HESS}}, \forall t = 1,...,T \tag{18}$$

$$P_{i,t}^{\mathrm{FC}} = \eta_i^{\mathrm{FC}} \times m_{i,t}^{\mathrm{FC}} \times \mathrm{LHV}; \quad \forall i \in \Omega_{\mathrm{HESS}}, \forall t = 1,...,T \tag{19}$$

Furthermore, the following constraint ensures that the electrolyzer and the fuel cell do not operate simultaneously at the same time:

$$u_{i,t}^{\mathrm{EL}} + u_{i,t}^{\mathrm{FC}} \le 1 \tag{20}$$

2.1.4 Battery energy storage system modeling

The mathematical model of the Battery Energy Storage System (BESS) is formulated as follows:

$$E_{i,0}^{\mathrm{BESS}} = \alpha_i^{\mathrm{BESS}} E_{\max,i}^{\mathrm{BESS}}; \quad \forall i \in \Omega_{\mathrm{BESS}} \tag{21}$$

$$E_{i,t}^{\mathrm{BESS}} = E_{i,t-1}^{\mathrm{BESS}} + \left[\eta^{\mathrm{BESS,ch}} P_{i,t}^{\mathrm{BESS,ch}} - \frac{1}{\eta^{\mathrm{BESS,dis}}} P_{i,t}^{\mathrm{BESS,dis}}\right]\Delta t; \quad \forall i \in \Omega_{\mathrm{BESS}}; t = 1,\ldots,T \tag{22}$$

$$\alpha_i^{\mathrm{BESS}} E_{\max,i}^{\mathrm{BESS}} \le E_{i,t}^{\mathrm{BESS}} \le E_{\max,i}^{\mathrm{BESS}}; \forall i \in \Omega_{\mathrm{BESS}}; \quad t = 1,\ldots,T \tag{23}$$

$$\begin{aligned} &0 \le P_{i,t}^{\mathrm{BESS,ch}} \le v_{i,t}^{\mathrm{BESS}} P_{\max,i}^{\mathrm{BESS}}; \qquad \forall i \in \Omega_{\mathrm{BESS}}; \quad t = 1,..,T \\ &0 \le P_{i,t}^{\mathrm{BESS,dis}} \le \left(1 - v_{i,t}^{\mathrm{BESS}}\right) P_{\max,i}^{\mathrm{BESS}}; \forall i \in \Omega_{\mathrm{BESS}}; \quad t = 1,..,T \end{aligned} \tag{24}$$

$$v_{i,t}^{\mathrm{BESS}} \in \{0,1\}; \quad \forall i \in \Omega_{\mathrm{BESS}}; \quad t = 1,\ldots,T \tag{25}$$

$$E_{i,0}^{\mathrm{BESS}} = E_{i,T}^{\mathrm{BESS}}; \forall i \in \Omega_{\mathrm{BESS}} \tag{26}$$

Equation (21) defines the initial state of the energy storage device. Constraint (22) tracks the energy level of the storage system at any time interval t. The allowable capacity of the storage unit is governed by (23), while constraint (24) restricts the charging and discharging power limits. To ensure that charging and discharging do not occur simultaneously, a binary variable $v_{i,t}$ is introduced in (25). Finally, expression (26) enforces the cyclic energy constraint, ensuring the energy levels at the beginning and the end of the scheduling period are identical.

2.2 Mixed integer second-order cone programming model

The power grid model in section 2.1 is formulated as a MINLP problem due to the nonlinear nature of constraints (2)–(7). To develop the MISOCP model, we define $I_{ij,t}^2 = I_{ij,t}^{\mathrm{sqr}}$ and $U_{i,t}^2 = U_{i,t}^{\mathrm{sqr}}$. Under these definitions, constraints (2)–(7) are transformed as follows:

$$\begin{aligned} &P_{i,t}^{\mathrm{sub}} + P_{i,t}^{\mathrm{DG}} + P_{i,t}^{\mathrm{FC}} - P_{i,t}^{\mathrm{EL}} - P_{i,t}^{\mathrm{D}} + P_{i,t}^{\mathrm{BESS,dis}} - P_{i,t}^{\mathrm{BESS,ch}} \\ &= \sum_{j \in \Phi_i, j \ne h} P_{ij,t} + R_{hi} \times I_{hi,t}^{\mathrm{sqr}} - P_{hi,t}; \forall i \in \Phi_{\mathrm{N}}; t = 1,\ldots,T \end{aligned} \tag{27}$$

$$Q_{i,t}^{\mathrm{sub}} + Q_{i,t}^{\mathrm{DG}} - Q_{i,t}^{\mathrm{D}} = \sum_{j \in \Phi_i, j \ne h} Q_{ij,t} + X_{hi} \times I_{hi,t}^{\mathrm{sqr}} - Q_{hi,t}; \quad \forall i \in \Phi_{\mathrm{N}}; t = 1,\ldots,T \tag{28}$$

$$U_{i,t}^{\mathrm{sqr}} - U_{j,t}^{\mathrm{sqr}} - 2\left(R_{ij} P_{ij,t} + X_{ij} Q_{ij,t}\right) + (R_{ij}^2 + X_{ij}^2) I_{ij}^{\mathrm{sqr}} = 0; \quad \forall ij \in \Phi_{\mathrm{L}}; t = 1,\ldots,T \tag{29}$$

$$I_{ij,t}^{\mathrm{sqr}} U_{i,t}^{\mathrm{sqr}} \ge P_{ij,t}^2 + Q_{ij,t}^2; \forall ij \in \Phi_{\mathrm{L}}; t = 1,\ldots,T \tag{30}$$

$$0 \le I_{ij,t}^{\mathrm{sqr}} \le I_{ij,\max}^2; \forall ij \in \Phi_{\mathrm{L}}; t = 1,\ldots,T \tag{31}$$

$$U_{i,\min}^2 \le U_{i,t}^{\mathrm{sqr}} \le U_{i,\max}^2; \forall i \in \Phi_{\mathrm{N}}; t = 1,\ldots,T \tag{32}$$

Constraint (5) is transformed from an equality into an inequality (30) to maintain the convex nature of the proposed MISOCP optimization framework.

After linearizing the non-linear constraints, the mixed-integer nonlinear programming model is reformulated as a second-order cone model. The final MISOCP model comprises the objective function (1) and the following sets of constraints:

− Power grid model: (27)–(32);
− HESS model: (8)–(20);
− BESS model: (21)–(26).

The MISOCP model of the problem can be efficiently solved to find the global optimal solution using mathematical solvers such as GUROBI, CPLEX, and XPRESS. **Figure 2** illustrates the algorithmic flowchart for solving the optimal operation problem of power grids integrated with hybrid energy storage systems.

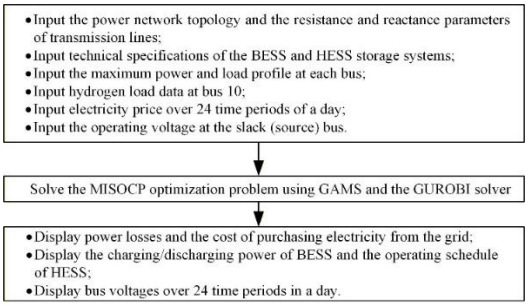

Figure 2: Flowchart of the proposed MISOCP method

3. Results and discussion

In this section, the proposed optimization model is implemented on the IEEE 33-bus radial distribution system [12]. The simulations are conducted within the GAMS modeling environment [13] using the GUROBI commercial solver. All numerical calculations are performed on a personal computer equipped with an AMD Ryzen 5 5600G (3.9 GHz) processor and 32 GB of RAM. The operating voltage at the substation (node 1) is set to 1 p.u.

3.1 Power grid data

The schematic of the modified IEEE 33-bus medium-voltage distribution system is illustrated in Figure 3. The nominal voltage of the grid is 12.66 kV. The total peak load demand is 3715 + *j*2300 kVA. The required voltage limits are set within $0.94 \le U \le 1.06$ per unit. The load characteristics at each node are presented in Table 1 [14]. Figure 4 depicts the daily load profiles for three different types of consumers with distinct patterns [15]. The electricity purchasing prices from the external grid are referred to [15]. The lifespan of both BESS and HESS is assumed to be 20 years, with a discount rate of 7%.

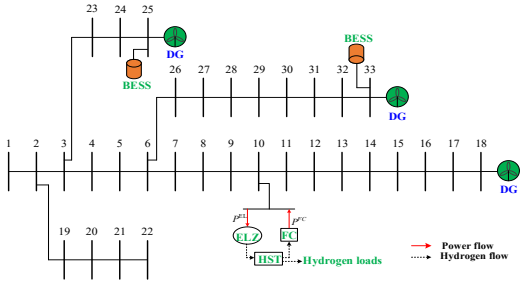

Figure 3: IEEE 33-bus medium-voltage distribution system

Distributed generation units are integrated at buses 18, 25, and 33. Each unit has an installed capacity of 1000 kVA and a power factor of $\cos\varphi = 0{,}95$. Figure 5 illustrates the forecasted power data (maximum power output) for these DG units [16].

Table 1: Load characteristics

Load type	Node
Residential	2, 5, 12, 14, 19, 22, 31, 32
Commercial	4, 7, 8, 10, 11, 13, 15, 17, 20, 23, 24, 25, 26, 28, 29, 30, 33
Industrial	3, 6, 9, 16, 18, 21, 27

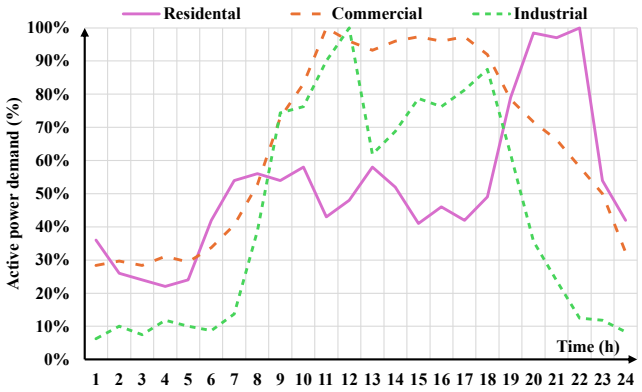

Figure 4: Daily load profiles

Figure 5: Forecasted power profiles of DGs (as % of installed capacity)

Table 2: HESS's technical specifications

Parameter	Value	Parameter	Value
LHV	3000 Wh/Nm^3	$\gamma_{\text{loss,HT}}$	0.001
$P^{\text{EL}}_{\text{max},i}$	2000 kW	$\eta^{\text{HT,in}}$	95%
$C^{\text{HT}}_{\text{ref},i}$	10000 kWh	$\eta^{\text{HT,out}}$	95%
$P^{\text{FC}}_{\text{max},i}$	2000 kW	α_i^{HT}	0.1
η_i^{EL}	85%	η_i^{FC}	75%
α_i^{EL}	0		

Battery energy storage systems (BESS) are installed at nodes 25 and 33. Both BESS units share the same technical specifications: a capacity of 2000 kWh, maximum charging/discharging power of 500 kW, minimum and maximum energy levels of 200 kWh and 2000 kWh, respectively, a charging/discharging efficiency of 90%, and an initial energy level of 200 kWh. The technical specifications of the HESS and the hydrogen load data at node 10 are presented in Table 2 and Table 3, respectively.

Table 3: Hydrogen load data at node 10

Hour	$m_{i,t}^{H2}\left(Nm^3/h\right)$	t	$m_{i,t}^{H2}\left(Nm^3/h\right)$	Hour	$m_{i,t}^{H2}\left(Nm^3/h\right)$
1	5	9	100	17	87.5
2	7.5	10	100	18	125
3	10	11	75	19	100
4	12.5	12	125	20	25
5	15	13	75	21	12.5
6	15	14	100	22	12.5
7	20	15	100	23	7.5
8	20	16	75	24	7.5

3.2 Numerical results

Two scenarios are evaluated and compared as follows:

– Scenario 1: Grid operation considering only the HESS.

– Scenario 2: Grid operation considering both the BESS and the HESS.

Table 4: Results for the two scenarios

Description	Scenario	
	1	2
Minimum operational voltage (p.u.)	0.96468	0.96889
Maximum operational voltage (p.u.)	1.06	1.06
Energy loss (kWh/day)	1,722.79	1,727.26
Electricity purchase cost from the transmission grid ($)	3,701,940.84	2,905,603.54

The calculation results of the objective function and other quantities for the two scenarios are presented in Table 4. This table illustrates significant differences between the two scenarios regarding voltage, energy loss, and electricity purchase costs from the transmission grid. The maximum voltage for both scenarios is identical, reaching 1.06 p.u. at bus 18. Additionally, there is a slight difference in the minimum voltage between the two scenarios. Specifically, the minimum voltage in Scenario 1 is 0.96468 p.u. (at bus 30, time t = 17), which is lower than that of Scenario 2, valued at 0.96889 p.u. (at bus 30, time t = 17).

Regarding daily energy losses, there is a slight difference between the two scenarios. The daily energy loss in Scenario 1 is 1,722.79 kWh, representing 3.28% of the load consumption. In Scenario 2, the daily energy loss accounts for 3.29% of the load consumption. The electricity purchase cost from the transmission grid shows a significant disparity between the two scenarios. The electricity purchase cost for Scenario 1 is $3,701,940.84, while the purchase cost for Scenario 2 is equivalent to 78.49% of that in Scenario 1.

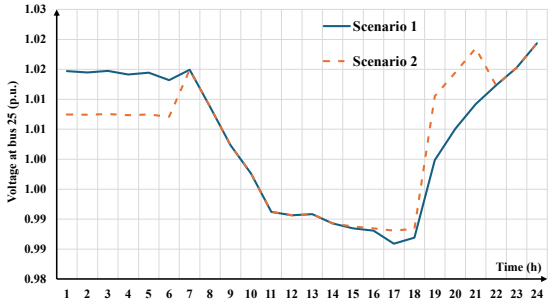

Figure 6: Voltage profile of node 25 over time

Figure 6 presents the voltage variations at bus 25 over a 24-hour horizon for the two scenarios. The maximum voltage values for both scenarios are identical, reaching 1.0193 p.u. at t = 24. However, the minimum voltage values at bus 25 differ between the two cases. In Scenario 1, the minimum voltage is 0.98590 p.u. at t = 17, while in Scenario 2, it is 0.98808 p.u. at the same time. From t = 1 to t = 6, the voltage at bus 25 in Scenario 1 is significantly lower than that in Scenario 2. Conversely, from t = 15 to t = 24, the voltage in Scenario 1 is higher than in Scenario 2. The voltage profiles across all network buses at t = 19 for both scenarios are illustrated in Figure 7. The peak voltages for Scenario 1 and Scenario 2 both occur at bus 18, with values of 1.04992 p.u. and 1.06000 p.u., respectively. The minimum voltages for both scenarios are observed at bus 22, recorded at 0.99643 p.u. and 0.99703 p.u., respectively. In general, the voltage levels at most buses in Scenario 2 are higher than those in Scenario 1.

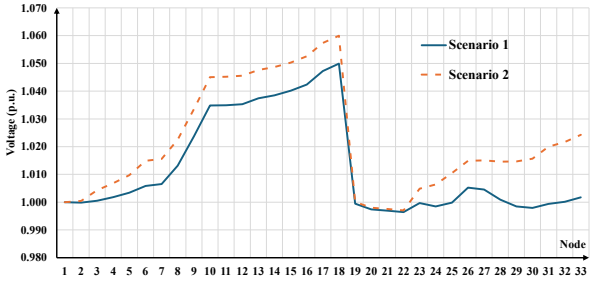

Figure 7: Comparison of node voltages of the power grid at t = 19

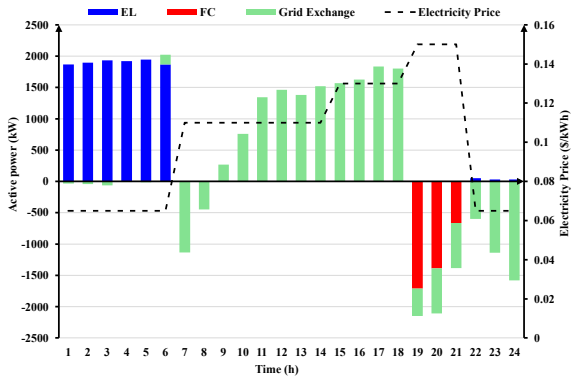

Figure 8: Operational schedule of the distribution grid in Scenario 1

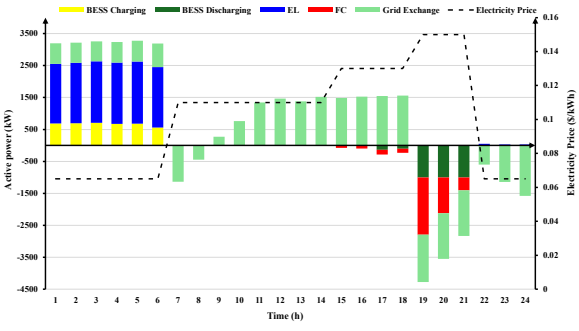

Figure 9: Operational schedule of the distribution grid in Scenario 2

Figure 8 presents the operational schedule of the distribution grid in Scenario 1. From t = 1 to t = 6, when the electricity price is at a low level (0.065 $/kWh), the electrolyzer operates continuously with an average power of approximately 1,905.85 kW and reaches a peak of 1,947.15 kW at t = 5. During this period, the distribution grid primarily utilizes electricity from distributed generation sources to produce hydrogen, while simultaneously selling a small

amount of electricity to the transmission grid. From $t = 7$ to $t = 8$, the system continues to sell electricity to the external grid with power levels of 1,133.20 kW and 448.51 kW, respectively. Subsequently, from $t = 9$ to $t = 18$, the distribution grid switches to purchasing a peak power value of 1,836.3 kW at $t = 17$. In the evening ($t = 19$–21), when the electricity price peaks at 0.15 \$/kWh, the fuel cell is activated to generate power with outputs of 1,711.48 kW, 1,389.37 kW, and 663.13 kW, respectively, helping to meet the load demand and sell electricity back to the transmission grid. As the electricity price decreases again (from $t = 22$ to $t = 24$), the FC ceases operation, the EL restarts at a low power level (30–50 kW), and the system continues to sell electricity to the external grid. The results demonstrate that the distribution grid operates flexibly according to electricity price fluctuations, contributing to energy balancing and enhancing economic efficiency.

Figure 9 presents the operational schedule of the distribution grid in Scenario 2. From $t = 1$ to $t = 6$, when the electricity price is low (0.065 \$/kWh), the electrolyzer operates continuously with an average power of approximately 1,905.84 kW to produce hydrogen. During this period, the BESS units charge with power ranging from 557.43 kW to 709.85 kW, while the distribution grid purchases electricity from the external grid with a power capacity of 622.80–736.59 kW. From $t = 7$ to $t = 8$, the EL and BESS cease operation, and the distribution grid sells electricity to the external grid with power levels of 1,133.20 kW and 449.51 kW, respectively. From $t = 9$ to $t = 18$, the grid switches to purchasing electricity from the transmission grid, with the purchased power increasing over time from 269.9 kW at $t = 9$ to a maximum value of 1,561.5 kW at $t = 18$. From $t = 15$ to $t = 18$, the fuel cell begins operating at a low power level, fluctuating between 78.98 kW and 148.81 kW, while the BESS discharges slightly to support the load. When the electricity price increases to 0.15 \$/kWh (from $t = 19$ to $t = 21$), the FC and BESS simultaneously generate power at high levels. Specifically, the FC outputs 1,794.3 kW, 1,119.1 kW, and 401.5 kW, respectively, while the BESS discharges at its maximum capacity of 1,000 kW throughout this period. The coordinated operation of the FC and BESS helps meet the load demand and sell electricity back to the transmission grid. From $t = 22$ to $t = 24$, as the electricity price decreases again, the FC stops operating, the EL restarts at a low power level (30–50 kW), and the grid continues to sell electricity externally.

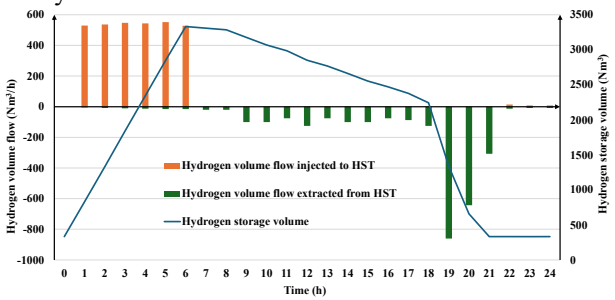

Figure 10: Optimal operational schedule of the hydrogen storage tank in Scenario 1

Figure 10 illustrates the optimal operational schedule of the hydrogen storage tank (HST) in Scenario 1. When electricity prices are low (from $t = 1$ to $t = 6$), the electrolyzer operates continuously to produce hydrogen, with the injection flow into the HST reaching its daily peak at $t = 6$. A portion of the hydrogen is stored in the tank, while the remainder is supplied to the system's hydrogen load demand. During periods of high electricity demand and peak prices (from $t = 19$ to $t = 21$), the fuel cell is activated, utilizing the stored hydrogen to generate power. This coordinated operation helps meet the load demand and reduces the amount of power purchased from the external grid. Following this stage, as electricity prices decrease, the EL is restarted to refill the HST, completing the 24-hour operational cycle.

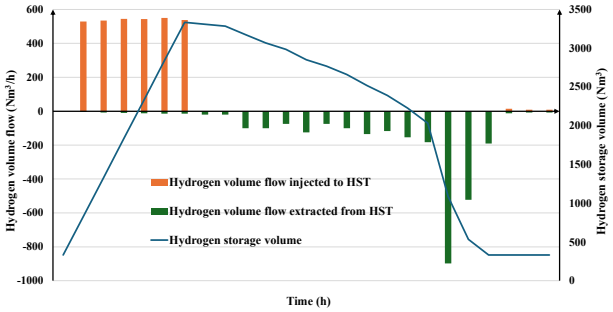

Figure 11: Optimal operational schedule of the hydrogen storage tank in Scenario 2

Figure 11 illustrates the optimal operational schedule of the hydrogen storage tank in Scenario 2, featuring the integrated operation of both HESS and BESS. Similar to Scenario 1, during the low electricity price period ($t = 1$–6), the electrolyzer operates intensively to produce hydrogen, leading the pressure within the HST to reach its maximum level at $t = 6$. A portion of the hydrogen is supplied to the load, while the remaining amount is stored for subsequent use. In contrast to Scenario 1, the hydrogen stored in the HST is discharged to the fuel cell for power generation earlier, specifically from $t = 15$ to $t = 21$. This strategy aims to support the BESS in meeting the load demand and further reducing electricity purchase costs. When the electricity price decreases ($t = 22$–24), the FC ceases operation, while the EL continues to refill the HST and supply the load, preparing for the next operational cycle.

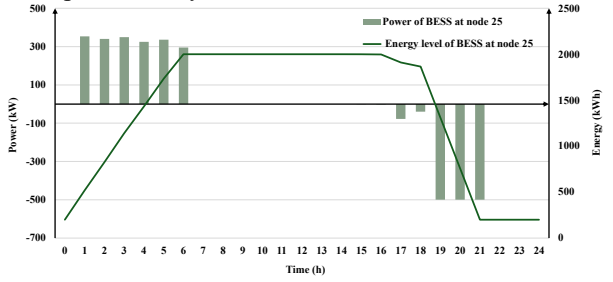

Figure 12: Operational behavior of the two BESS at bus 25

Figure 12 and Figure 13 illustrate the operational behavior of the two BESS at buses 25 and 33 over a 24-hour period in Scenario 2. The operational strategy of these BESS units is contingent upon the load demand and the fluctuating electricity prices exchanged with the transmission grid. Specifically, during periods of low load demand and electricity prices (from $t = 1$ to $t = 6$), the devices tend to charge to store energy. Conversely, when load demand and prices increase ($t = 17$ to $t = 21$), the BESS units discharge power back into the grid. As a result, the energy level of the BESS at bus 25 reaches its maximum between $t = 6$ and $t =$

14, with a total daily energy of 34,491 kWh. Similarly, the BESS at bus 33 maintains its maximum energy level from t = 6 to t = 15, totaling 34,548 kWh for the day. This charging/discharging strategy highlights the effective use of BESS in cost optimization and grid support.

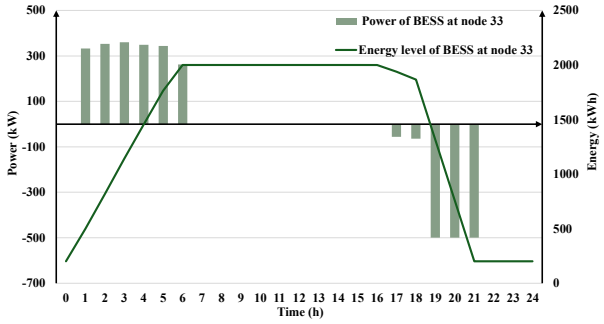

Figure 13: Operational behavior of the two BESS at bus 33

3.3 SOCP relaxation accuracy

The second-order cone relaxation is employed to convexify the power balance constraints. To verify the accuracy of the model transformation, the maximum relaxation error at each time interval is calculated using the defined formula and is presented in Figure 14. The results indicate that the peak maximum error is 29.68×10^{-7} (occurring at t = 17). This demonstrates that the convexification process does not introduce significant discrepancies between the two sides of the constraints. Consequently, the convexified model remains equivalent to the original nonlinear model, confirming the accuracy of the proposed model transformation.

$$g_t = \max\left\{\left|I^{\mathrm{sqr}}_{ij,t}U^{\mathrm{sqr}}_{i,t} - P^2_{ij,t} - Q^2_{ij,t}\right|\right\};\ \forall ij \in \Phi_{\mathrm{L}};\ t = 1,\ldots,T \qquad (33)$$

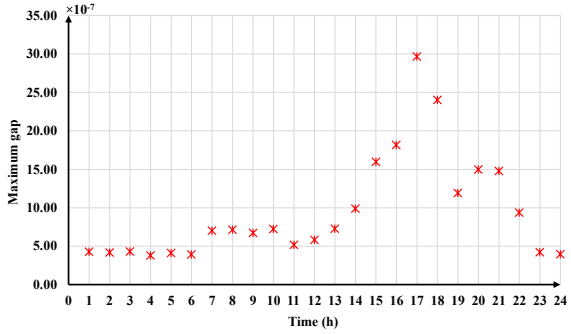

Figure 14: Maximum SOCP relaxation gap

4. Conclusions

This study presents a mixed-integer second-order cone programming (MISOCP) model for the optimal operation of a distribution grid integrated with a hybrid energy storage system. The model considers distributed generation and daily load profiles, with an objective function aimed at minimizing the costs of electricity exchanged with the transmission grid. The proposed model was applied to a modified IEEE 33-bus system. The results demonstrate that the integration of both BESS and HESS systems is highly effective, yielding a 21.51% reduction in power exchange costs compared to the scenario using only the HESS. Operational results also show that the BESS and HESS units charge and discharge flexibly, charging during low-price periods and discharging during peak-price intervals. This operational strategy enables the distribution grid to effectively adapt to the variability of distributed generation resources. Future research will focus on expanding the proposed MISOCP framework to include demand-side management (DSM) programs to further enhance grid flexibility. Additionally, the model can be extended to analyze large-scale, unbalanced distribution networks to better reflect real-world operating conditions. Another significant direction involves investigating the long-term degradation effects of BESS and HESS components, as their life-cycle costs play a critical role in the overall economic feasibility. Finally, the authors plan to incorporate the uncertainty of load demand and renewable energy resources to ensure the robustness of the optimal operation strategy.

Acknowledgement

This work was supported by the Hanoi University of Science and Technology (HUST) under the Grant T2024-PC-065.

References

[1] S. Jeon and S. Bae, "Integrated optimization for sizing, placement, and energy management of hybrid energy storage systems in renewable power systems," *J. Energy Storage*, vol. 106, p. 114793, Jan. 2025, doi: 10.1016/j.est.2024.114793.

[2] T. Gu *et al.*, "Placement and capacity selection of battery energy storage system in the distributed generation integrated distribution network based on improved NSGA-II optimization," *J. Energy Storage*, vol. 52, p. 104716, Aug. 2022, doi: 10.1016/j.est.2022.104716.

[3] A. Bouaouda and Y. Sayouti, "An optimal sizing framework of a microgrid system with hydrogen storage considering component availability and system scalability by a novel approach based on quantum theory," *J. Energy Storage*, vol. 92, p. 111894, July 2024, doi: 10.1016/j.est.2024.111894.

[4] G. Carpinelli, C. Noce, A. Russo, P. Varilone, and P. Verde, "Optimal siting and sizing of battery energy storage systems in unbalanced distribution systems: A multi objective problem under uncertainty," *Int. J. Electr. Power Energy Syst.*, vol. 162, p. 110316, Nov. 2024, doi: 10.1016/j.ijepes.2024.110316.

[5] Z. Medghalchi and O. Taylan, "A novel hybrid optimization framework for sizing renewable energy systems integrated with energy storage systems with solar photovoltaics, wind, battery and electrolyzer-fuel cell," *Energy Convers. Manag.*, vol. 294, p. 117594, Oct. 2023, doi: 10.1016/j.enconman.2023.117594.

[6] T. Gangwar, N. P. Padhy, and P. Jena, "Storage Allocation in Active Distribution Networks Considering Life Cycle and Uncertainty," *IEEE Trans. Ind. Inform.*, vol. 19, no. 1, pp. 339–350, Jan. 2023, doi: 10.1109/TII.2022.3167382.

[7] F. Serra, M. Lucariello, M. Petrollese, and G. Cau, "Optimal Integration of Hydrogen-Based Energy Storage Systems in Photovoltaic Microgrids: A Techno-Economic Assessment," *Energies*, vol. 13, no. 16, p. 4149, Aug. 2020, doi: 10.3390/en13164149.

[8] Z. Mojaradi, R. Tavakkoli-Moghaddam, A. Bozorgi-Amiri, and J. Heydari, "A two-stage risk-based framework for dynamic configuration of a renewable-based distribution system considering demand response programs and hydrogen storage systems," *Int. J. Hydrog. Energy*, vol. 62, pp. 256–271, Apr. 2024, doi: 10.1016/j.ijhydene.2024.03.073.

[9] L. Wen and W. Jiang, "Bi-level capacity optimization of electricity-hydrogen coupled energy system considering power curtailment constraint and technological advancement," *Energy*, vol. 307, p. 132603, Oct. 2024, doi: 10.1016/j.energy.2024.132603.

[10] N. S. Attemene, K. S. Agbli, S. Fofana, and D. Hissel, "Optimal sizing of a wind, fuel cell, electrolyzer, battery and supercapacitor

system for off-grid applications," *Int. J. Hydrog. Energy*, vol. 45, no. 8, pp. 5512–5525, Feb. 2020, doi: 10.1016/j.ijhydene.2019.05.212.

[11] S. Seyyedeh-Barhagh, M. Majidi, S. Nojavan, and K. Zare, "Optimal Scheduling of Hydrogen Storage under Economic and Environmental Priorities in the Presence of Renewable Units and Demand Response," *Sustain. Cities Soc.*, vol. 46, p. 101406, Apr. 2019, doi: 10.1016/j.scs.2018.12.034.

[12] S. H. Dolatabadi, M. Ghorbanian, P. Siano, and N. D. Hatziargyriou, "An Enhanced IEEE 33 Bus Benchmark Test System for Distribution System Studies," *IEEE Trans. Power Syst.*, vol. 36, no. 3, pp. 2565–2572, May 2021, doi: 10.1109/TPWRS.2020.3038030.

[13] *GAMS Documentation 46*. (Feb. 17, 2024). GAMS Development Corp. Accessed: Feb. 25, 2026. [Online]. Available: https://www.gams.com

[14] M. R. Dorostkar-Ghamsari, M. Fotuhi-Firuzabad, M. Lehtonen, and A. Safdarian, "Value of Distribution Network Reconfiguration in Presence of Renewable Energy Resources," *IEEE Trans. Power Syst.*, vol. 31, no. 3, pp. 1879–1888, May 2016, doi: 10.1109/TPWRS.2015.2457954.

[15] S. S. F. Souza, R. Romero, J. Pereira, and J. T. Saraiva, "Artificial immune algorithm applied to distribution system reconfiguration with variable demand," *Int. J. Electr. Power Energy Syst.*, vol. 82, pp. 561–568, Nov. 2016, doi: 10.1016/j.ijepes.2016.04.038.

[16] A. Kumar *et al.*, "Strategic integration of battery energy storage systems with the provision of distributed ancillary services in active distribution systems," *Appl. Energy*, vol. 253, p. 113503, Nov. 2019, doi: 10.1016/j.apenergy.2019.113503.